Delving into Process–Microstructure–Property Relationships in Cast-Extruded Polylactic Acid/Talc Composite Films: Effect of Different Screw Designs

Journal of
Composites Science

MDPI

Article

Delving into Process–Microstructure–Property Relationships in Cast-Extruded Polylactic Acid/Talc Composite Films: Effect of Different Screw Designs

Giulia Bernagozzi [1,2], Chiara Gnoffo [1,2], Rossella Arrigo [1,2,*] and Alberto Frache [1,2]

[1] Department of Applied Science and Technology, Politecnico di Torino, Viale Teresa Michel, 15121 Alessandria, Italy; giulia.bernagozzi@polito.it (G.B.); chiara.gnoffo@polito.it (C.G.); alberto.frache@polito.it (A.F.)
[2] Local INSTM Unit, 15121 Alessandria, Italy
* Correspondence: rossella.arrigo@polito.it

Abstract

In the context of polymer-based composites, the knowledge of the correlations between the processing conditions, the microstructure, and the final properties is essential to tailor polymeric systems for specific applications. Specifically concerning the extrusion process, an accurate design of the screw profile allows for achieving composites with modulable microstructures, according to the specific properties required by the intended application. In this work, films of polylactic acid-based composites with 5 wt.% of talc were obtained by means of a single-screw extruder equipped with a flat die and a calender unit. Three different screw profiles, namely a general-purpose compression screw, a screw with a reverse flow zone, and a barrier screw, were employed for the production of films. The ability of the screw profile in varying the degree of filler dispersion and distribution was assessed through morphological and rheological analyses, demonstrating that the barrier screw is more able in disaggregating the talc lamellae. Due to the achieved microstructures, films produced using this screw profile exhibited superior barrier properties, with a decrease of about 27% in the oxygen permeability as compared to unfilled PLA. However, a concurrent decrease in material ductility as compared to the other films was observed. Finally, the thermoformability of the composites was assessed; also in this case, trays with more precise edges and corners were obtained for the film formulated through the barrier screw.

Keywords: single-screw extruder; screw profile; cast extrusion; oxygen permeability; thermoforming

Academic Editor: Heitor Luiz Ornaghi Júnior

Received: 30 July 2025
Revised: 26 August 2025
Accepted: 2 September 2025
Published: 4 September 2025

Citation: Bernagozzi, G.; Gnoffo, C.; Arrigo, R.; Frache, A. Delving into Process–Microstructure–Property Relationships in Cast-Extruded Polylactic Acid/Talc Composite Films: Effect of Different Screw Designs. *J. Compos. Sci.* **2025**, *9*, 483. https://doi.org/10.3390/jcs9090483

1. Introduction

In the field of plastic packaging, polylactic acid (PLA) is the most widely used biopolymer, owing to its biodegradability, non-toxicity when in contact with food, and adaptability to different processing technologies for the production of different plastic goods and items [1–3]. Moreover, by introducing different types of fillers, several specific properties can be achieved in PLA-based composites, such as high oxygen permeability or increased mechanical performances [4,5]. However, in polymer-based composites, the achievement of a homogeneous dispersion and distribution of the embedded fillers, leading to the establishment of a great polymer/filler interfacial region, is a mandatory requirement for obtaining materials endowed with superior properties [6,7]. When polymer-based composites are formulated through melt-compounding technologies, the conditions selected for

the processing (namely, temperature profile, screw design, feed rate, and screw rotation speed) play a key role in determining the extent of dispersion and/or distribution of the embedded fillers [8]. For this reason, the co-rotating twin-screw extruder (TSE) is the most widely exploited equipment for the effective compounding of thermoplastics-based systems, including blends, composites, and nanocomposites. In fact, in TSE, both dispersive and distributive mixing are applied, with the design of the screws enabling the balancing of these two effects depending on the desired morphology of the compounded materials. However, at the industrial level, the most widespread types of equipment for the production of plastic goods are single-screw extruders (SSE), which constitute the fundamental part of different technologies, such as blow molding and the formulation of pipes, profiles, flat films, and coated wires, among a few to mention. Moreover, single-screw extruders enable large throughputs, despite their generally low mixing efficiency due to the non-uniform shear rate and melt temperature distribution generally observed in such equipment [9,10]. This limitation severely restricts the effective use of single-screw extruders in large-scale compounding and blending operations. In order to overcome this intrinsic limitation, several screw designs have been proposed for enhancing mixing efficiency in SSE [11,12]. Furthermore, the effects of screw geometries on output rate, melting, and pressure profile have been extensively studied, and several models to predict the processing features have been developed [13,14].

From a general point of view, the control of the final microstructure of a polymer-based composite (governed by the processing conditions), including filler dispersion, distribution, and interfacial bonding between the matrix and the reinforcement, is a crucial factor in determining the ultimate properties of the material [15]. In particular, considering applications such as packaging, oxygen permeability represents a critical property. As widely reported in the literature, lamellar fillers or nanofillers (such as talc and nanoclays, respectively) are very effective in increasing the diffusion path of the gas through the material, causing a decrease in the oxygen transmission rate as compared to the unfilled polymer [16–18]. In this context, it has been demonstrated that talc particles are able to reduce permeability in packaging composites [19–21]. In particular, the materials' final performances are strictly affected by some inherent filler characteristics, such as particle size, aspect ratio, and superficial area [19].

Nevertheless, also in this case, the microstructure of the composite plays a significant role in controlling the barrier properties, since the diffusion of gases within the material depends on both the degree of dispersion of the fillers and the crystallinity degree of the system [16].

Although some studies focused on correlating the final properties with the changes in the processing parameters [22–24], few works are dedicated to exploring the correlation between the morphology and the properties when varying the screw design employed in single-screw extrusion processes.

In this work, three different screw configurations were exploited for formulating PLA-based films containing 5 wt.% of talc, aiming at evaluating the possible effect of the different screw designs on the material morphology and related properties, while maintaining unchanged the processing parameters. Rheological, thermal, mechanical, and barrier properties were assessed as a function of the screw configuration, demonstrating the ability of the screw profile to affect the final morphology and thus the final properties. Moreover, the thermoforming ability of the PLA-based composites processed with the three different screw profiles was evaluated by shaping the films into a typical tray for packaging applications.

2. Materials and Methods

2.1. Materials

Film Grade PLA 4042D (92% L-lactide and 8% D-lactide units, polydispersity index = 2, density = 1.25 g/cm^3) produced by NatureWorks® Ingeo™ was used as a matrix, while IMI Fabi HTP1 talc was employed as a filler (D_{50} = 1.9 μm, D_{98} = 8.0 μm, density = 2.8 g/cm^3, specific surface area (SSA) = 10 m^2/g).

2.2. Processing

Both PLA and talc have been dried at 80 and 100 °C overnight, respectively. First, a masterbatch of PLA-based composite containing 25 wt.% of talc was obtained through a corotating twin-screw extruder LEISTRITZ (Nürnberg, Germany) ZSE 18 HP (screw diameter 18 mm, barrel length 720 mm, L/D = 40). The barrel temperature and screw speed have been set at 190 °C and 150 rpm, respectively, with a flow rate equal to 700 g/h.

The so-obtained PLA-based masterbatch has been then diluted and extruded as films using an EUR.EX.MA Srl (Varese, Italy) single-screw extruder (D = 25 mm, L/D = 32) equipped with a flat die and a calender unit (three rolls, d1 = 150 mm, d2,3 = 220 mm). Films of PLA + 5 wt.% talc (hereinafter named as PLA + T) with a thickness ranging from 150 to 250 μm were achieved and used for further characterization. Three different screw configurations (reported in Figure S1 in Supplementary Materials) were exploited for formulating the films: a conventional three-compression-zone screw, a screw with a reverse flow zone, and a barrier screw, hereinafter named C-screw, R-screw, and B-screw, respectively. Regardless of the type of screw used, the barrel temperature during the extrusion was set to 190 °C and the screw speed to 40 rpm. The rolls of the calender unit were cooled to 25 °C.

In order to obtain trays, a micro thermoforming machine (TFM) (EUR.EX.MA Srl, Varese, Italy) equipped with a squared mold was used (mold geometry reported in Figure S2). The thermoforming machine is heated through an infrared oven, which allows temperatures up to 250 °C with a maximum working time limit of 200 s.

2.3. Characterization Techniques

An ARES (TA Instruments, New Castle, DE, USA) rotational plate–plate rheometer was employed to perform frequency sweep tests at 190 °C, at frequencies ranging from 100 to 0.1 rad/s in a nitrogen atmosphere. Rheological measurements were carried out within the linear viscoelastic range of each sample (preliminarily determined through strain sweep tests). The complex viscosity curves as a function of the frequency have been fitted by using the Cross model (Equation (1)) [25]:

$$\eta^*(\omega) = \eta_0 \cdot \left[\frac{1}{1+(k\omega)^m}\right] \quad (1)$$

where η_0 is the zero-shear viscosity, ω is the frequency, k is the average relaxation time, and m is an exponent describing the level of non-Newtonian behavior.

A Zeiss (Oberkochen, Germany) EVO 15 Scanning Electron Microscope (SEM) (20 kV beam voltage and 8.5 mm working distance) was used for morphological inspections of films preliminarily covered with a sputtered gold layer, after achieving brittle fracture of the samples through immersion in liquid nitrogen. ImageJ (Version 1.54p, Bethesda, MD, USA) image analysis software was used to elaborate SEM micrographs.

The thermal tests were performed with a DSC (Differential Scanning Calorimetry) TA Q20 (TA Instruments, New Castle, DE, USA). Three runs (heating–cooling–heating) were performed from 0 °C to 250 °C with a heating/cooling rate of 10 °C/min in a continuous nitrogen flow. The glass transition temperature (T_g), crystallization temperature

(T_C), cold crystallization temperature (T_{CC}), melting temperature (T_M), crystallization enthalpy (ΔH_C), cold crystallization enthalpy (ΔH_{CC}), and melting enthalpy (ΔH_M) were evaluated. The crystallinity degree of PLA and PLA + 5 wt% talc was assessed by using Equation (2) [26]:

$$\chi_C = \frac{\Delta H}{\left(\Delta H_M^0 \cdot \varphi PLA\right)} \cdot 100 \quad (2)$$

where $\Delta H = \Delta H_M - \Delta H_{CC}$, ΔH_M^0 is the melting enthalpy of 100% crystalline PLA (93 J/g [22]), and φPLA is the polymer content.

To assess the oxygen transmission rate (OTR), used to obtain oxygen permeability (OP) normalized by the thickness of the films, the Multiperm Extra Solution (Master Lab, Milano, Italy) instrument was employed. The permeability tests were carried out at 23 °C with relative humidity equal to 0%, a film area of 50 cm^2, and an initial conditioning time of one hour for every 10 µm of film thickness. The test was concluded when the collected data achieved an OTR accuracy within 0.5%. OTR and OP values were calculated by using Equations (3) and (4) [27]:

$$OTR = \frac{volume\ O_2}{area * day * pressure} \quad (3)$$

$$OP = OTR * film\ thickness \quad (4)$$

Finally, tensile testing was carried out by using a 5966 Instron (Norwood, MA, USA) dynamometer equipped with a 2 kN load cell and 250 N clamps on die-cut rectangular-shaped specimens (90 × 10 mm), with the speed set at 1 mm/min. Tensile tests were performed on at least 5 specimens for each material, and the results were averaged.

3. Results and Discussion

3.1. Effect of the Screw Profile on the Morphology of PLA + T Films

Figure 1 depicts the SEM micrographs of PLA + T films formulated by using the screw characterized by the three-compression zone (Figure 1a), reverse flow zone (Figure 1b), and barrier zone (Figure 1c). The processing with the C-screw and the R-screw results in both quite good dispersion and distribution of talc. Furthermore, the embedded fillers are well-oriented along the flow direction, owing to the application of the elongational flow during the processing for the production of the films [28]. The average length of talc lamellae (both individually dispersed and stacked) reported in Table 1 is almost comparable for the films obtained with both screw profiles. A noticeably better distribution of talc within the matrix occurs when the B-screw is used for the processing. In particular, as testified by the lower value of the average dimension reported in Table 1, lamellae (and/or stacks) with smaller equivalent diameters are observed as compared to the films produced with the other two screw profiles. This result is in agreement with what was already demonstrated by the work of Ariño et al. [29], in which the better efficiency of the barrier screw in disaggregating filler clusters is highlighted. However, the processing of the PLA + T composite with the B-screw leads to a loss of filler orientation, resulting in smaller, well-dispersed but disordered talc lamellae.

Table 1. Average dimension of talc lamellae in PLA-based composite films.

Sample	Average Dimension [µm]
PLA + T_C-screw	3.2 ± 0.98
PLA + T_R-screw	2.7 ± 1.26
PLA + T_B-screw	1.4 ± 0.75

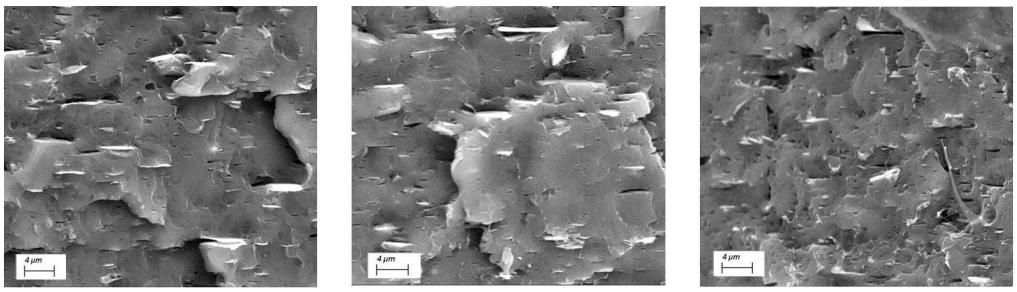

Figure 1. SEM micrographs of PLA + T_C-screw (**a**), PLA + T_R-screw (**b**), and PLA + T_B-screw (**c**).

Figure 2 reports the complex viscosity curves of all produced films, including unfilled PLA and composites. From a general point of view, the rheological behavior of PLA is affected by the presence of talc but also by the screw profile.

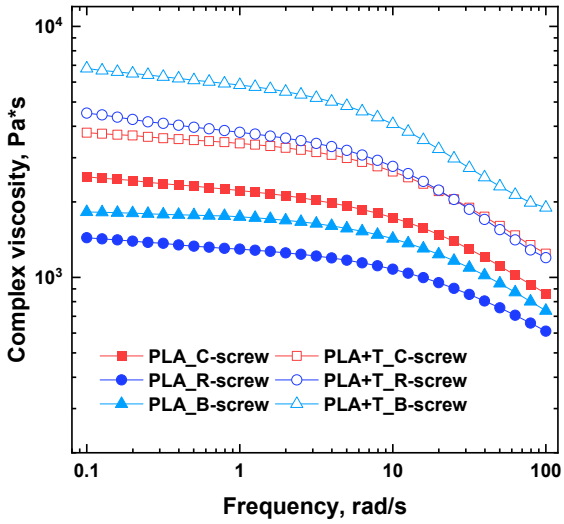

Figure 2. Complex viscosity curves of neat PLA and PLA + T composites processed with C-screw, R-screw, and B-screw.

Regardless of the screw profile employed for the extrusion, the complex viscosity curves of the pristine PLA are characterized by a Newtonian plateau at low frequencies and a mild shear thinning behavior in the high-frequency region, as anticipated by other authors [30]. Concerning the effect of the screw geometry on the unfilled matrix, some differences can be noticed. In particular, pristine PLA processed with both B- and R-screws exhibits lower values of complex viscosity over the entire frequency range with respect to PLA_C-screw. This result can be explained by considering that during the processing the polymer is subjected to relatively high thermal and shear stresses, inducing some degradation phenomena that cause a decrease in the polymer molecular weight [31]. To further investigate this issue, the values of the zero-shear viscosity (η_0) of the samples were derived by fitting the experimental data with the Cross model (Equation (1)). In fact, it has been widely reported [31,32] that a decrease in η_0 may indicate the occurrence of chain scission reactions, resulting in a decrease in the molecular weight. The obtained values of η_0 (reported in Table 2) clearly depend on the screw type: the highest η_0 was obtained for the C-screw, followed by the B-screw and R-screw, respectively.

Table 2. Zero-shear viscosity values for unfilled PLA films.

Sample	η_0 [Pa*s]
PLA_C-screw	2507
PLA_R-screw	1427
PLA_B-screw	1839

Therefore, there is a pronounced effect of the screw design on the structural degradation of PLA, which suffers a decrease in the molecular weight and, thus, more intense degradation phenomena when the melt processing is carried out with the barrier screw and even more with the R-screw if compared to the standard compression screw. The reason behind this phenomenon likely lies in the high residence time when the B-screw and R-screw are exploited, due to the sections containing the reverse flow and barrier elements that delay the advancing of the polymer melt.

Considering the PLA-based composites, irrespective of the screw design, the incorporation of talc results in an overall increase in the complex viscosity as compared to unfilled PLA, according to the literature [31,33].

Nevertheless, some interesting differences emerge when comparing the behavior of the composites produced using the different screws.

In particular, for the composites obtained through C-screw and R-screw, very similar values of the complex viscosity were obtained. However, considering the viscosities of the corresponding unfilled matrices, the processing with the R-screw led to an amplification of the effect of talc on the complex viscosity values as compared to the C-screw. This behavior is better highlighted in Figure 3, where the ratio between the complex viscosity of the talc-containing films and that of the unfilled PLA processed with the same screw profile is reported.

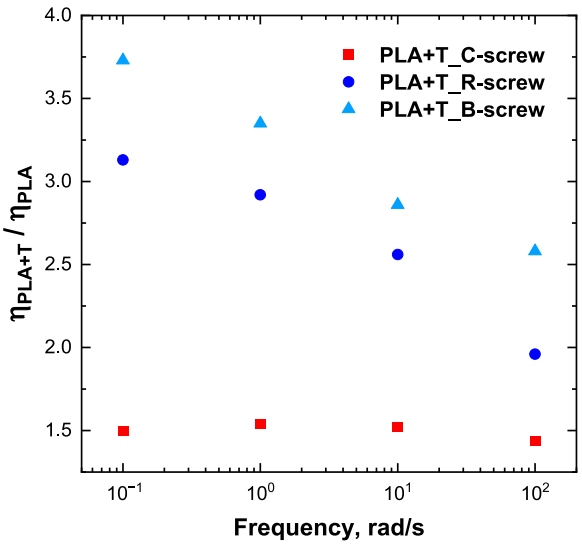

Figure 3. Ratio between the complex viscosity of the talc-containing films and that of the unfilled PLA processed with the same screw profile as a function of the frequency.

As clearly observed, in the whole tested frequency interval, the increment of the viscosity induced by the introduction of talc is higher for the R-screw-processed material, indicating the better efficiency of this screw profile (likely due to the presence of the reverse flow zone) in promoting the dispersion and distribution of the embedded fillers as compared to the C-screw.

On the other hand, considering the B-screw, the processing with this screw profile involves an even more remarkable growth of the complex viscosity of the composite

with respect to the unfilled PLA_B-screw. In fact, the increase in the complex viscosity when talc is added within PLA is the highest among the three investigated systems. This phenomenon can be ascribed to the impact of the barrier screw profile on the filler dispersion/distribution, leading to talc lamellae with smaller dimensions and better distribution, as already highlighted by SEM observations.

Furthermore, looking at the data reported in Figure 3, it is evident that in the composites processed through the R- and B-screws, the ratio between the viscosities of the composite and of the matrix tends to increase with decreasing frequency, while for the materials obtained through the C-screw, the behavior is practically constant over the frequency.

This result further confirms what was inferred about the enhanced degree of dispersion of the embedded filler in R- and B-screw processed films. In fact, the more pronounced non-Newtonian behavior in the low-frequency region for these materials, as compared to the respective unfilled matrices, can be associated with a restriction of chain relaxation dynamics due to the well-dispersed talc lamellae that are able to establish some interactions with the polymer macromolecules [34].

3.2. Thermal, Mechanical, and Oxygen Permeability Properties of PLA + T Films

Table 3 displays the thermal properties evaluated from the DSC thermograms recorded during the first heating (reported in Figure S3) and the cooling for the unfilled PLA and the composites extruded with the three different screws. Although the final crystallinity content and the characteristic temperatures are poorly affected by both the introduction of talc and the screw geometry, some interesting effects can be highlighted.

Table 3. Main thermal properties for all investigated PLA and PLA + T films.

Specimen	T_g (°C)	ΔH_{CC} (J/g)	T_{M1} (°C)	T_{M2} (°C)	ΔH_M (J/g)	χ_C (%)	ΔH_C (J/g)
PLA_C-screw	60.0	-	152.7	-	6.9	7.4	-
PLA_R-screw	55.5	-	152.2	-	7.8	8.4	-
PLA_B-screw	59.4	-	151.9	-	8.4	8.9	-
PLA + T_C-screw	58.9	20.4	147.3	153.2	24.9	5.1	1.6
PLA + T_R-screw	59.3	21.6	148.2	154.3	26.2	5.2	1.7
PLA + T_B-screw	59.9	21.1	146.9	152.9	27.2	6.8	1.9

More specifically, the glass transition temperature of unfilled PLAs processed with the different screws shows some differences, with the lowest value obtained with the R-screw. This result confirms what has already been inferred through rheological analysis about possible degradation phenomena taking place during the processing. In fact, according to the Fox–Flory theory [31,35], the decrease in T_g could be ascribed to a decrease in the molecular weight of PLA_R-screw due to the chain scission reactions occurring during the processing, as already demonstrated by the decrease in the zero-shear viscosity for this sample. However, this difference is no longer observable in the talc-containing films, which exhibit comparable T_g regardless of the screw designs.

Differently, the incorporation of talc influences either the cold crystallization phenomenon or the melting transition. In particular, differently from the unfilled PLA samples, all the composite films exhibit cold crystallization, likely due to the nucleation effect of the embedded talc, as widely documented in the literature [36,37]. Moreover, for the talc-containing films, a crystallization peak, which is not present in the unfilled PLA thermogram, was observed during the cooling cycle. On the other hand, during the first heating ramp, a secondary endothermic peak appears at lower temperatures with respect to the melting peak of unfilled PLAs. The presence of this multiple melting peak can be attributed

to heterogeneous nucleation phenomena and the consequent formation of two different crystalline species [38]. Concerning the crystallinity content, the introduction of talc causes a slight decrease as compared to pristine PLAs, likely due to some disruption phenomena occurring within the matrix, which are caused by the finely dispersed lamellae [39].

The effects of the screw geometry on the mechanical properties and oxygen permeability have been investigated as well.

The tensile stress–strain curves of PLA-based films processed with the three different screws are plotted in Figure 4, while the main mechanical properties (mean values and standard deviations of elastic modulus, maximum tensile strength, and elongation at break) are listed in Table 4, alongside those of the unfilled PLA.

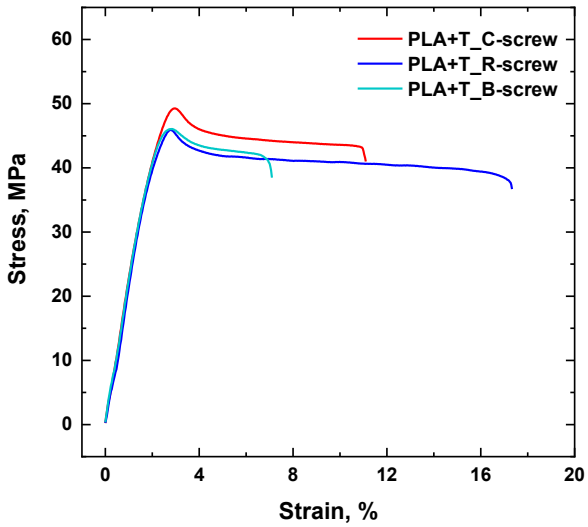

Figure 4. Stress–strain curves for all investigated PLA + T films.

Table 4. Main mechanical properties for all investigated PLA + T films (the properties of a representative PLA film sample are also reported).

Specimen	Elastic Modulus (MPa)	Tensile Strength (MPa)	Elongation at Break (%)
PLA + T_C-screw	2102 ± 100	49.2 ± 0.8	9.5 ± 1.3
PLA + T_R-screw	2133 ± 153	46.7 ± 1.0	14.1 ± 3.3
PLA + T_B-screw	2341 ± 190	47.1 ± 1.2	6.1 ± 0.9
PLA	2042 ± 103	45.3 ± 1.1	11.6 ± 1.9

As far as the pristine matrix is concerned, the screw profile does not affect the mechanical behavior, and all three samples exhibit practically unchanged values of the main tensile properties. In fact, in Table 4 the properties of a representative PLA film sample are reported. According to the literature [37,40], the introduction of talc causes an increase in the elastic modulus and a slight rise of the tensile stress values as compared to the unfilled PLA. Among the different PLA + T films, the sample processed through the B-screw shows a more brittle behavior; in fact, it presents the highest value of elastic modulus and reduced deformability. The increased rigidity can be explained considering that the evaluation of the material morphology highlighted for this sample the achievement of smaller talc lamellae and better filler distribution with respect to the other films. As a result, an increased filler/matrix interfacial area is expected to develop in this material, guaranteeing a more efficient stress transfer mechanism from the matrix to the talc particles during external loading [40].

The higher deformability of the PLA + T_R-screw sample with respect to unfilled PLA is quite surprising. In fact, usually the introduction of talc results in a decrease in

the matrix elongation at break, as for instance documented in the literature for injection-molded PLA/talc composites [41]. The results obtained in this work could be explained by considering that, due to the application of the elongational flow during the film production, either the PLA macromolecules or the talc particles show a preferential orientation along the stretching direction. This phenomenon, as already demonstrated for polymer-based nanocomposites, alleviates the stress concentration around the embedded fillers, thereby facilitating the material deformation [42].

Concerning the barrier properties of the formulated films (see the values of oxygen permeability reported in Table 5), as expected, the introduction of talc induced a decrease in the oxygen permeability as compared to the unfilled PLA, due to the more tortuous pathway for the gas diffusion in the presence of the filler [16]. Looking at the results obtained for the talc-containing materials, the PLA + T_B-screw sample presents slightly decreased oxygen permeability compared to the other two films. As before demonstrated by morphological and rheological analyses, for this composite, smaller, well-dispersed but disordered talc lamellae were obtained. As reported by Bharadwaj [43], in polymer-based composites and nanocomposites, the gas permeability strictly depends on the extent of dispersion and distribution of the embedded fillers. In fact, better filler disaggregation and their more homogeneous distribution within the polymeric matrix promote an increasing ability in delaying the diffusion of the oxygen molecules through the film. On the other hand, it has been shown that also the orientation of high aspect ratio fillers affects the tortuosity of the gas pathway through the film; in particular, lower permeability values are usually obtained when the embedded particles have a random orientation within the polymer matrix [44]. Therefore, the obtained results can be associated with the composite morphology, which in turn has been demonstrated to be strictly governed by the processing conditions imposed during the film preparation.

Table 5. Oxygen transmission rate (OTR) and oxygen permeability (OP) for all investigated PLA + T films (the properties of a representative PLA film sample are also reported).

Specimen	Film Thickness (μm)	OTR (cc/(m^2 × 24 h))	OP (cc/(m^2 × 24 h) × mm)
PLA_C-screw	220	75.6	16.6
PLA_R-screw	180	86.5	15.6
PLA_B-screw	160	90.9	14.5
PLA	160	123.6	19.8

3.3. Thermoformability Assessment

Several trials have been performed on composite films processed with the three different screw profiles in order to evaluate their thermoformability. For all the films, initially the lamp of the thermoforming apparatus was warmed up for 90 s; subsequently, four trays in sequence have been obtained for each sample. Figures S4–S6 report some representative pictures of the produced items. Overall, it can be noticed that all PLA + T films showed adequate thermoformability, notwithstanding some defects in the final trays, especially for the films processed with C- and R-screws. Figure 5 reports some representative pictures of one of the most critical points of the thermoformed item, namely the edges and sides, which tend to deform after the demolding step. It can be noticed that more satisfactory results were achieved with the PLA + T_B-screw film, which allowed for achieving more defined angles, while the other thermoformed items are characterized by less sharply defined edges.

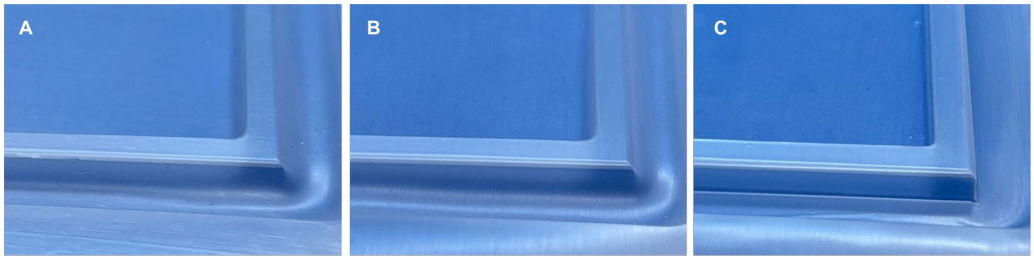

Figure 5. Representative pictures of a detail of the thermoformed trays obtained using (**A**) PLA + T_C-screw, (**B**) PLA + T_R-screw, and (**C**) PLA + T_B-screw.

4. Conclusions

Aiming at disclosing fundamental relationships between the processing conditions, the material morphology, and the resulting properties, PLA + T films were produced through a single-screw extruder equipped with a flat die and a calender unit by employing three different screw profiles. The analysis of the films' microstructure revealed that the barrier screw was more effective in disaggregating the talc lamellae and in achieving a more disordered arrangement of the fillers within the polymer matrix. Otherwise, the films produced using C-screw and, especially, R-screw exhibited a well-recognizable preferential orientation of the talc particles along the film direction. The different observed morphologies impacted the final properties of the films in different ways. More specifically, the increased talc disaggregation and the formation of a disordered filler arrangement in the PLA + T_B-screw sample promoted the achievement of lower oxygen permeability values for this sample (namely, 14.5 cc/(m^2·24 h)·mm), likely due to the formation of more tortuous pathways for the gas diffusion. On the other hand, the good extent of filler dispersion and distribution obtained by using the R-screw and, especially, the preferential orientation of the talc lamellae along the film production direction induced an increase of about 21% of the deformability for the composite film formulated with this screw as compared to unfilled PLA.

Finally, all the investigated PLA + T films demonstrated adequate thermoformability. In fact, trays with a low level of defects were obtained with all the materials, despite the slightly superior quality of the items produced starting from the B-screw processed films.

Supplementary Materials: The following supporting information can be downloaded at: https://www.mdpi.com/article/10.3390/jcs9090483/s1. Figure S1. Screw profiles; Figure S2. Tray mold design; Figure S3. DSC thermograms recorded during the first heating scan for PLA and talc-containing composites processed with the different screw profiles; Figure S4. Pictures of the trays thermoformed using the film PLA + T_C-screw; Figure S5. Pictures of the trays thermoformed using the film PLA + T_R-screw; Figure S6. Pictures of the trays thermoformed using the film PLA + T_B-screw.

Author Contributions: Conceptualization, A.F.; methodology, A.F. and R.A.; formal analysis, G.B. and C.G.; investigation, G.B. and C.G.; writing—original draft preparation, G.B. and C.G.; writing—review and editing, A.F. and R.A.; supervision, A.F. and R.A. All authors have read and agreed to the published version of the manuscript.

Funding: This research received no external funding.

Data Availability Statement: Datasets are available on request from the authors.

Conflicts of Interest: The authors declare no conflicts of interest.

References

1. Conn, R.E.; Kolstad, J.J.; Borzelleca, J.F.; Dixler, D.S.; Filer, L.J.; Ladu, B.N.; Pariza, M.W. Safety assessment of polylactide (PLA) for use as a food-contact polymer. *Food Chem. Toxicol.* **1995**, *33*, 273–283. [CrossRef]
2. Abdelshafy, A.; Hermann, A.; Herres-Pawlis, S.; Walther, G. Opportunities and Challenges of Establishing a Regional Bio-based Polylactic Acid Supply Chain. *Glob. Chall.* **2023**, *7*, 2200218. [CrossRef]
3. Malek, N.S.A.; Faizuwan, M.; Khusaimi, Z.; Bonnia, N.N.; Rusop, M.; Asli, N.A. Preparation and Characterization of Biodegradable Polylactic Acid (PLA) Film for Food Packaging Application: A Review. *J. Phys. Conf. Ser.* **2021**, *1892*, 012037. [CrossRef]
4. Snowdon, M.R.; Wu, F.; Mohanty, A.K.; Misra, M. Comparative study of the extrinsic properties of poly(lactic acid)-based biocomposites filled with talc versus sustainable biocarbon. *RSC Adv.* **2019**, *9*, 6752–6761. [CrossRef]
5. Helanto, K.; Talja, R.; Rojas, O.J. Effects of talc, kaolin and calcium carbonate as fillers in biopolymer packaging materials. *J. Polym. Eng.* **2021**, *41*, 746–758. [CrossRef]
6. Arrigo, R.; Malucelli, G. Rheological Behavior of Polymer/Carbon Nanotubes Composites: An Overview. *Materials* **2020**, *13*, 2771. [CrossRef]
7. Thostenson, E.K.; Ren, Z.; Chou, T.W. Advances in the science and technology of carbon nanotubes and their composites: A review. *Compos. Sci. Technol.* **2001**, *61*, 1899–1912. [CrossRef]
8. D'Anna, A.; Arrigo, R.; Frache, A. Rheology, morphology and thermal properties of a PLA/PHB/clay blend nanocomposite: The influence of process parameters. *J. Polym. Environ.* **2022**, *30*, 102–113. [CrossRef]
9. Wilczynski, K.; Lewandowski, A.; Wilczynski, K.J. A composite model for starve fed single screw extrusion of thermoplastics. *Polym. Eng. Sci.* **2012**, *52*, 1258. [CrossRef]
10. Gaspar-Cunha, A.; Costa, P.; Delbem, A.; Monaco, F.; Ferreira, M.J.; Covas, J. Evolutionary Multi-Objective Optimization of Extrusion Barrier Screws: Data Mining and Decision Making. *Polymers* **2023**, *15*, 2212. [CrossRef]
11. Kelly, A.L.; Brown, E.C.; Coates, P.D. The effect of screw geometry on melt temperature profile in single screw extrusion. *Polym. Eng. Sci.* **2006**, *46*, 1706–1714. [CrossRef]
12. Kazmer, D.O.; Grosskopf, C.M.; Rondeau, D.; Venoor, V. Design and Evaluation of General Purpose, Barrier, and Multichannel Plasticating Extrusion Screws. *Polym. Eng. Sci.* **2020**, *60*, 752–764. [CrossRef]
13. Xiao, K.; Tzoganakis, C. An experimental study of single-screw extrusion of HDPE–wood composites. *Adv. Polym. Technol.* **2010**, *29*, 197–218. [CrossRef]
14. Wilczyński, K.; Buziak, K.; Wilczyński, K.; Lewandowski, A.; Nastaj, A. Computer Modeling for Single-Screw Extrusion of Wood–Plastic Composites. *Polymers* **2018**, *10*, 295. [CrossRef]
15. Bernagozzi, G.; Arrigo, R.; Frache, A. Evolution of the Microstructure of PP-LDHs Nanocomposites during Melt Compounding: A Simulation Approach. *Polymers* **2023**, *16*, 70. [CrossRef]
16. Trinh, B.M.; Chang, B.P.; Mekonnen, T.H. The barrier properties of sustainable multiphase and multicomponent packaging materials: A review. *Prog. Mater. Sci.* **2023**, *133*, 101071. [CrossRef]
17. Wolf, C.; Angellier-Coussy, H.; Gontard, N.; Doghieri, F.; Guillard, V. How the shape of fillers affects the barrier properties of polymer/non-porous particles nanocomposites: A review. *J. Membr. Sci.* **2018**, *556*, 393–418. [CrossRef]
18. Cui, Y.; Kumar, S.; Rao Kona, B.; van Houcke, D. Gas barrier properties of polymer/clay nanocomposites. *RSC Adv.* **2015**, *5*, 63669–63690. [CrossRef]
19. Habibi, K.; Castejón, P.; Martínez, A.B.; Arencón, D. Effect of filler content, size, aspect ratio and morphology on thermal, morphological and permeability properties of porous talc filled—Polypropylene obtained through MEAUS process. *Adv. Polym. Technol.* **2018**, *37*, 3315–3324. [CrossRef]
20. Nath, D.; Pal, A.K.; Misra, M.; Mohanty, A.K. Biodegradable Blown Film Composites from Bioplastic and Talc: Effect of Uniaxial Stretching on Mechanical and Barrier Properties. *Macromol. Mater. Eng.* **2023**, *308*, 2300214. [CrossRef]
21. Gryta, M. The Influence of Talc Addition on the Performance of Polypropylene Membranes Formed by TIPS Method. *Membranes* **2019**, *9*, 63. [CrossRef]
22. Furlan, L.G.; Ferreira, C.I.; Dal Castel, C.; Santos, K.S.; Mello, A.C.E.; Liberman, S.A.; Oviedo, M.A.S.; Mauler, R.S. Effect of processing conditions on the mechanical and thermal properties of high-impact polypropylene nanocomposites. *Mater. Sci. Eng. A* **2011**, *528*, 6715–6718. [CrossRef]
23. Lertwimolnun, W.; Vergnes, B. Influence of screw profile and extrusion conditions on the microstructure of polypropylene/organoclay nanocomposites. *Polym. Eng. Sci.* **2007**, *47*, 2100–2109. [CrossRef]
24. Racca, L.M.; Pacheco, E.B.A.V.; Bertolino, L.C.; Campos, C.X.S.; Andrade, M.C.; Sousa, A.M.F.; Silva, A.L.N. Composites Based on Polypropylene and Talc: Processing Procedure and Prediction Behavior by Using Mathematical Models. *Adv. Condens. Matter Phys.* **2018**, *2018*, 6037804. [CrossRef]
25. Nichetti, D.; Manas-Zloczower, I. Viscosity model for polydisperse polymer melts. *J. Rheol.* **1998**, *42*, 951–969. [CrossRef]
26. Battegazzore, D.; Bocchini, S.; Frache, A. Crystallization kinetics of poly(lactic acid)-talc composites. *Express Polym. Lett.* **2011**, *5*, 849–858. [CrossRef]

27. Battegazzore, D.; Alongi, J.; Frache, A. Poly(lactic acid)-Based Composites Containing Natural Fillers: Thermal, Mechanical and Barrier Properties. *J. Polym. Environ.* **2014**, *22*, 88–98. [CrossRef]
28. Arrigo, R.; Malucelli, G.; La Mantia, F.P. Effect of the elongational flow on the morphology and properties of polymer systems: A brief review. *Polymers* **2021**, *13*, 3529. [CrossRef]
29. Ariño, R.; Boldizar, A. Barrier Screw Compounding and Mechanical Properties of EAA Copolymer and Cellulose Fiber Composite. *Int. Polym. Process.* **2013**, *28*, 421–428. [CrossRef]
30. Nofar, M.; Salehiyan, R.; Sinha Ray, S. Rheology of poly (lactic acid)-based systems. *Polym. Rev.* **2019**, *59*, 465–509. [CrossRef]
31. Cuadri, A.A.; Martín-Alfonso, J.E. Thermal, thermo-oxidative and thermomechanical degradation of PLA: A comparative study based on rheological, chemical and thermal properties. *Polym. Degrad. Stab.* **2018**, *150*, 37–45. [CrossRef]
32. Bernagozzi, G.; Arrigo, R.; Ponzielli, G.; Frache, A. Towards effective recycling routes for polypropylene: Influence of a repair additive on flow characteristics and processability. *Polym. Degrad. Stab.* **2024**, *223*, 110714. [CrossRef]
33. Huang, A.; Yu, P.; Jing, X.; Mi, H.-Y.; Geng, L.-H.; Chen, B.-Y.; Peng, X.-F. The Effect of Talc on the Mechanical, Crystallization and Foaming Properties of Poly(Lactic Acid). *J. Macromol. Sci. Part B* **2016**, *55*, 908–924. [CrossRef]
34. Zhang, Q.; Fang, F.; Zhao, X.; Li, Y.; Zhu, M.; Chen, D. Use of Dynamic Rheological Behavior to Estimate the Dispersion of Carbon Nanotubes in Carbon Nanotube/Polymer Composites. *J. Phys. Chem. B* **2008**, *112*, 12606–12611. [CrossRef]
35. Rasselet, D.; Ruellan, A.; Guinault, A.; Miquelard-Garnier, G.; Sollogoub, C.; Fayolle, B. Oxidative degradation of polylactide (PLA) and its effects on physical and mechanical properties. *Eur. Polym. J.* **2014**, *50*, 109–116. [CrossRef]
36. Rocca-Smith, J.R.; Karbowiak, T.; Marcuzzo, E.; Sensidoni, A.; Piasente, F.; Champion, D.; Heinz, O.; Vitry, P.; Bourillot, E.; Lesniewska, E.; et al. Impact of corona treatment on PLA film properties. *Polym. Degrad. Stab.* **2016**, *132*, 109–116. [CrossRef]
37. Yu, F.; Liu, T.; Zhao, X.; Yu, X.; Lu, A.; Wang, J. Effects of talc on the mechanical and thermal properties of polylactide. *J. Appl. Polym. Sci.* **2012**, *125*, E99–E109. [CrossRef]
38. Jain, S.; Misra, M.; Mohanty, A.K.; Ghosh, A.K. Thermal, Mechanical and Rheological Behavior of Poly(lactic acid)/Talc Composites. *J. Polym. Environ.* **2012**, *20*, 1027–1037. [CrossRef]
39. Wang, T.; Liu, D.; Keddie, J.L. An alternative approach to the modification of talc for the fabrication of polypropylene/talc composites. *J. Appl. Polym. Sci.* **2007**, *106*, 386–393. [CrossRef]
40. Leong, Y.W.; Abu Bakar, M.B.; Ishak, Z.A.M.; Ariffin, A.; Pukansky, B. Comparison of the Mechanical Properties and Interfacial Interactions Between Talc, Kaolin, and Calcium Carbonate Filled Polypropylene Composites. *J. Appl. Polym. Sci.* **2004**, *91*, 3315–3326. [CrossRef]
41. Petchwattana, N.; Covavisaruch, S.; Petthai, S. Influence of talc particle size and content on crystallization behavior, mechanical properties and morphology of poly(lactic acid). *Polym. Bull.* **2014**, *71*, 1947–1959. [CrossRef]
42. La Mantia, F.P.; Ceraulo, M.; Mistretta, M.C.; Sutera, F.; Ascione, L.; Nasillo, G. Effect of elongational flow and polarity of organomodified clay on morphology and mechanical properties of a PLA based nanobiocomposite. *Int. Polym. Process.* **2016**, *31*, 541–547. [CrossRef]
43. Bharadwaj, R.K. Modeling the barrier properties of polymer-layered silicate nanocomposites. *Macromolecules* **2001**, *34*, 9189–9192. [CrossRef]
44. Choudalakis, G.; Gotsis, A.D. Permeability of polymer/clay nanocomposites: A review. *Eur. Polym. J.* **2009**, *45*, 967–984. [CrossRef]